CHALMERS

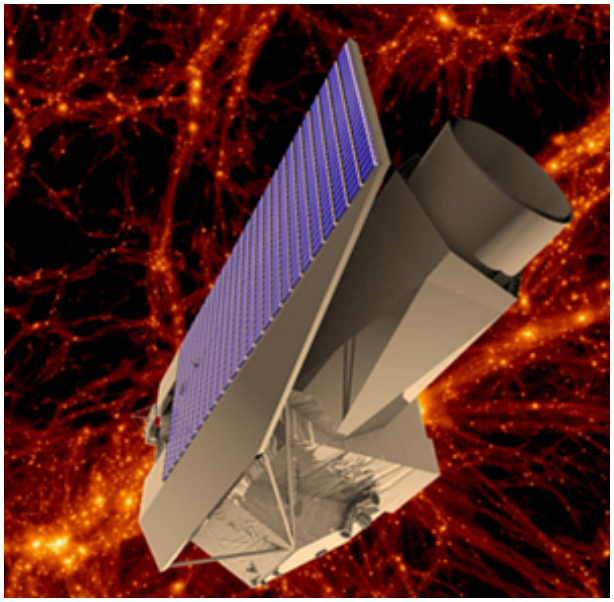

Estimating masses of galaxy clusters

a first step in exploring dark matter

Master of Science Thesis in the Fundamental Physics program

Elisabet Liljeblad

Department of Earth and Space Sciences
Chalmers University of Technology
Gothenburg, Sweden, 2012

Primary supervisor: Kristian Pedersen
Consultants and collaborators: Radek Wojtak and Andreas Skielboe

University of Copenhagen
Niels Bohr Institute, Dark Cosmology Center

Examiner: Magnus Thomasson

Chalmers University of Technology

Contents

Acknowledgements

I would like to express my appreciation to my advisors during my time in Copenhagen writing my thesis: Kristian Pedersen, Radek Wojtak and Magnus Thomasson. Special thanks to Kristian Pedersen, my supervisor who was the one who gave me the opportunity to do my Master's thesis at Dark Cosmology Center in Copenhagen and to be a part of the Euclid project. He has welcomed me into Dark in a way that made me feel comfortable and appreciated, and has been patient, understanding and very helpful. I also want to thank Radek Wojtak for spending time in helping and advising me in my work, and for making me feel comfortable and at home at Dark. Finally I would like to thank Magnus Thomasson, my advisor in Gothenburg at Chalmers University of Technology, who has especially helped me in finalizing my thesis.

Abstract

Masses of galaxy clusters and the cluster mass function (abundance of clusters as a function of cluster masses), have been estimated from the largest cluster catalog of SDSS galaxies using mainly three different interloper removal methods: the maximum velocity approach, the 2-3σ-clipping approach and the maximum velocity gap approach. In these three approaches the virial mass estimator have been used. The maximum velocity approach sets a criteria on the circular velocity and the infalling velocity for every galaxy in a certain distance to the cluster center. The 2-3σ-clipping approach cuts off interlopers by using the standard deviation on the velocities of the galaxies. Finally, the maximum velocity gap approach sets a constraint on the absolute velocity difference between neighboring galaxies. A set of 200 clusters provided by Wang et al. (2012) has been simulated on. The maximum velocity approach with a velocity constraint of 3000 km/s agrees best with the mass function derived analytically in Klypin et al. (2011). When using Hubble's law, this constraint yields to a maximum cluster radii of around 40 Mpc (in the same range as the superclusters). The 2σ-clipping approach also agrees well with the mass function in Klypin et al. (2011). However it is clear that when there is an excess of interlopers or too few member galaxies in the cluster, all three methods give a larger uncertainty and become less qualitative.

The mass function derived is to be used as a forecasting tool for the European Space Agency mission Euclid.

1 Introduction

A background of the project as well as method and goal is provided for the reader as an introduction.

1.1 Background

Galaxy clusters are the largest known gravitationally bound objects in the universe. They are particularly interesting for studying large-scale physical processes, the cosmic evolution of the intergalactic intracluster medium (ICM) and the structure and evolution of our universe. The galaxy clusters can be used as probes of structure and galaxy formation as they retain an imprint of how they were formed. As dark matter affects clusters, they are also valuable for measuring dark matter in the universe (Böhringer & Werner 2010). The determination of the mass function, the abundance of galaxy clusters as a function of their mass, is particularly important for constraining cosmological models. The present-day cluster mass function was the first observation to suggest that the standard $\Omega_m = 1$ Cold Dark Matter (CDM) model must be very biased in order to match the observed abundance of clusters (Bahcall et al. 2000).

The aim of the thesis is to provide a mass function by the use of different interloper[1] removal methods and two mass estimators. The interlopers in the clusters have a substantial effect on the mass estimation of the cluster. Therefore it is utterly important to find an interloper removal method that take enough galaxies into account and removes all the outlying galaxies.

The clusters analysed are from the SDSS (Sloan Digital Sky Survey) catalog[2] and the Gaussian Mixture Brightest Cluster Galaxy (GMBCG) galaxy cluster catalog. The reason for finding a mass function is to use it as a forecasting tool for how well data from the space telescope mission Euclid will be able to make cluster mass estimations.

Euclid mission Euclid is a European Space Agency space telescope mission, planned to be launched in 2019. The ambition of Euclid is to provide the next quantum leap in our understanding of dark matter and dark energy. The mission will provide a map of the universe 75 times larger than any current data available, make homogeneous sampling of galaxies and provide dark energy constraints. Taking galaxies and clusters out to redshift 2 into account in a wide extragalactic survey covering 15 000 deg^2 and a deep survey covering an area of 40 deg^2, the total effective volume of Euclid will be 19.7 Gpc^{3}h^{-3}. The wavelength will be in the visible and the near-infrared. Euclid will measure around 50 million galaxy redshift and 60 000 clusters between $z = 0.2$ and $z = 2.0$ (Laureijs et al. 2011).

[1] Interlopers when considering clusters of galaxies are galaxies which do not belong to a specific cluster because of their positions relative to the cluster core or their velocities.

[2] The SDSS LRG (Luminous Red Galaxies) catalog have a total effective volume of 0.26 Gpc^{3}h^{-3}. The SDSS catalog is the largest volume of the universe currently mapped.

1.2 Method and goals

The goals of this thesis is to investigate mass estimators for SDSS clusters and to provide a mass function with the use of relevant interloper removal methods and mass estimators. The purpose of finding a mass function is to use it as a forecasting tool for how well the data from the ESA mission Euclid will be able estimate cluster masses and thus a cluster mass function.

2 Theory and Methods

This section includes the virial theorem, two mass estimators, an analytic expression of the mass function, how to calculate the galaxy velocities with respect to the cluster center, the distance between stellar objects, the overdensity mass, a MATLAB and bootstrapping section and a section describing the procedure for estimating the cluster mass function.

2.1 Virial Theorem

The virial theorem states that if a spherical distribution of objects of equal mass is stable and self-gravitating (such as a galaxy cluster), the total gravitational potential energy (U) of the objects is equal to minus two times the total kinetic energy (T):

$$U = -2T \Rightarrow \frac{1}{2} G \frac{M_{\text{total}}^2}{R_{\text{total}}} = M_{\text{total}} v^2 \tag{1}$$

$$M_{\text{total}} \approx 2 \frac{R_{\text{total}} v^2}{G} \tag{2}$$

where v^2 is the mean of the squares of velocities of the objects, M_{total} is the total mass of the objects, R_{total} is a measure of the size of the system and G is the gravitational constant. The system needs to be in equilibrium, which means that the system is only allowed to change slowly over some relevant timescale (Dibai et al. 1959).

2.2 Mass Estimators

There are many ways to estimate masses of galaxy clusters. In this thesis the two mass estimators virial mass and projected mass will be used. The virial mass is often used as an estimator of mass inside a dark matter halo. If a region in space has a relatively large number of galaxies one can assume that they have been there for a long time, and thus the virial theorem can be applied. The projected mass is generally less accurate than the virial mass and considers the average quantity of the velocity times the radius to the cluster center for each cluster member.

In the interloper removal algorithm virial mass projected mass ratio approach (see section 3.2.5) the ratio of the projected mass and virial mass is used. The projected mass is generally more sensitive to interlopers than the virial mass is.

2.2.1 Virial Mass

Assuming that the virial theorem applies, the system is self-gravitating and the bodies in the system have equal masses, the virial mass estimator is usually written as:

$$M_{\text{v}}(r = R_{\text{max}}) = \frac{3\pi N}{2G} \frac{\sum_i (v_i - \bar{v})^2}{\sum_{i<j} 1/R_{\perp ij}} \tag{3}$$

where N is the number of cluster members enclosed on the sky by a circle with radius R_{max}, v_i is the line of sight velocity relative to the center of the cluster for the i:th galaxy, $\bar{v}$ is the mean of all

the galaxy velocities and $R_{\perp ij} = |R_{\perp i} - R_{\perp j}|$ is the projected separation between the two galaxies i and j. The virial mass is thus given by summing up for every R_i in increasing order (Heisler et al. 1985).

2.2.2 The Projected Mass

When the virial theorem applies, the projected mass estimator can be used. This estimator uses the average of the quantity $v_z^2 r_\perp$ over all the galaxies in a cluster:

$$M_{\rm p} = \frac{f_{\rm p}}{GN} \sum_i v_{zi}^2 r_{\perp i} \tag{4}$$

where N is the number of cluster members, $r_\perp$ is the projected separation from the cluster center and v_z is the line of sight velocity relative to the cluster center. The constant $f_{\rm p}$ depends on the distribution of orbits. According to Heisler et al. (1985), in the absence of specific information about the distribution of orbit eccentricities the recommended value of $f_{\rm p}$ is $32/\pi$.

2.3 Mass function by Klypin et al.

The article by Klypin et al. (2011) provides an analytic expression for the mass function by using the ST approximation (Sheth & Tormen 2001). It presents results from the Bolshoi dissipationsless cosmological $\wedge$CDM-simulation[3], and uses statistics of halos and subhalos to present an accurate approximation for the halo mass function:

$$M\frac{dn}{dM} = \Omega_{\rm m,0}\rho_{\rm crit,0}\frac{d\sigma(M)}{\sigma(M)dM}f(\sigma) = 2.75 \cdot 10^{11}(h^{-1}Mpc)^{-3}\Omega_{\rm m,0}h^2\frac{M_{\rm sun}d\sigma}{\sigma dM}f(\sigma) \tag{5}$$

where M is the halo virial mass, n is the cumulative velocity function[4], $\Omega_{\rm m,0}(= 0.27)$ is the density contribution of matter at $z = 0$, $\rho_{\rm crit,0}$ is the critical density and $f(\sigma)$ and σ can be approximated

[3]The Bolshoi simulation was run in a volume 250 h^{-1}Mpc on a side using around 8 billion particles with mass and force resolution adequate to follow subhalos down to the completeness limit of $v_{\rm circular}$ = 50 km/s maximum circular velocity.

[4]The velocity function for cluster halos declining very steeply with velocity:

$$n(>V) = AV^{-3}\exp\Big(-\frac{V}{V_0}^{\alpha}\Big) \tag{6}$$

where the parameters A, V_0 and α are functions of redshift:

$$\begin{aligned} A &= 1.52 \cdot 10^4 \sigma_8^{-3/4}(z)(h^{-1}{\rm Mpc/kms^{-1}})^{-3}, \\ \alpha &= 1 + 2.15\sigma_8^{4/3}(z), \\ V_0 &= 3000\frac{\sigma_8^2(z)}{1 + 2.5\sigma_8^2(z)}{\rm km/s} \end{aligned} \tag{7}$$

σ_8 is the root-mean-square mass fluctuation in spheres with radius $8h^{-1}$Mpc. The velocities are ranging from 50-1000 km/s.

by the following expressions (Klypin et al. 2011):

$$f(\sigma) = A\sqrt{\frac{2b}{\pi}}\Big(1 + (bx^2)^{-0.3}\Big)x\exp\Big(-\frac{bx^2}{2}\Big)$$
$$x \equiv \frac{1.686}{\sigma(M)}, \quad A = 0.322, \quad b = 0.707 \tag{8}$$

$$\sigma(M) = \frac{16.9y^{0.41}}{1 + 1.102y^{0.20} + 6.22y^{0.333}}$$
$$y \equiv \Big(\frac{M}{10^{12}h^{-1}M_{\rm sun}}\Big)^{-1} \tag{9}$$

where $h = 0.72$. This approximation has an accuracy of more than 2% for masses $M > 10^7 h^{-1} M_{\rm sun}$.

2.4 Galaxy velocities with respect to cluster center

One needs to be careful when determining velocities of galaxies in a cluster as they are calculated in a less simple way than $V = c \cdot z$. The results can be applied to any cosmological receding object that has a peculiar velocity. The redshift is given by:

$$z = (\lambda - \lambda_{\rm G})/\lambda_{\rm G} \tag{10}$$

where $\lambda_{\rm G}$ is the wavelength of radiation emitted by the galaxy and λ is the corresponding observed wavelength. Ignoring gravitational redshift corrections, the observed redshift consists of three components. The first is z_0, the Doppler shift due to the radial component v_0 of our own peculiar velocity as measured by a local observer O moving with the expanding universe. The second and third contributions are the cosmological redshift $z_{\rm R}$ and the Doppler shift $z_{\rm G}$ from the radial component of $v_{\rm G}$ of the observed galaxy. They are calculated as:

$$1 + z_0 = \sqrt{\frac{c - v_0}{c + v_0}} \tag{11}$$

$$1 + z_{\rm R} = \frac{\lambda_0}{\lambda_{\rm R}} \tag{12}$$

$$1 + z_{\rm G} = \sqrt{\frac{c + v_{\rm G}}{c - v_{\rm G}}} \tag{13}$$

which together gives:

$$1 + z = (1 + z_0)(1 + z_{\rm R})(1 + z_{\rm G}) \tag{14}$$

It is fairly common to ignore the contribution of z_0 to z, as z_0 tends to be much smaller. At the same time substituting $v_{\rm rad} = c \cdot z_{\rm G}$ for the line of sight velocity of the galaxy with respect to the cluster center, one gets:

$$v_{\rm rad} = c \cdot \frac{z - z_{\rm R}}{1 + z_{\rm R}} \tag{15}$$

Further letting z_{R} correspond to the mean redshift of the sample, z_{cluster}, and z correspond to the measured redshift for each cluster member, z_{galaxy}, the equation for the radial velocity is (Harrison 1974):

$$v_{\mathrm{rad}} = c \cdot \frac{z_{\mathrm{galaxy}} - z_{\mathrm{cluster}}}{1 + z_{\mathrm{cluster}}} \tag{16}$$

2.5 Spherical Law of Cosines and Distance Between Galaxies and Clusters

In order to calculate the distance between to objects on the sky, such as the distance between two galaxies or the distance between one galaxy and the cluster center, the spherical law of cosines needs to be applied, see Weisstein (2012):

$$\cos(A) = \sin(d_1) \cdot \sin(d_2) + \cos(d_1) \cdot \cos(d_2) \cdot \cos(|r_1 - r_2|) \tag{17}$$

where d_1, d_2, r_1 and r_2 are the declination (Dec) and right ascension (RA) of two different objects in the sky, respectively, and A is the spherical distance between the two objects. Further the equation for the calculation of the distance between these two objects becomes:

$$d = \tan(A) \cdot D_{\mathrm{cluster}} \tag{18}$$

where D_{cluster} is the distance between Earth and the cluster center.

2.6 Overdensity

The spherical overdensity mass of a galaxy cluster is defined as the mass within the radius R_Δ enclosing a given density contrast Δ with respect to some reference density ρ_{crit}. The spherical overdensity mass and radius are related by (Tinker et al. 2008):

$$M_\Delta = \frac{4\pi}{3} \rho_{\mathrm{crit}} R_\Delta^3 \Delta \tag{19}$$

where

$$\rho_{crit} = \frac{3H_0^2}{8\pi G} \tag{20}$$

Here Δ denotes a multiple of the critical density ρ_{crit} and H_0 is the Hubble constant. The choice of reference Δ is quite arbitrary. However in this thesis, $\Delta = 200$ is chosen, which is near 178, the overdensity at which a spherically symmetric sphere of matter virializes (Tittley & Couchman 1999).

2.7 MATLAB

The programming of the interloper removal methods was made from scratch using the computing language and interactive environment MATLAB. The built-in functions polyfit and polyval were used for making polynomial fitting of curves. MATLAB's own bootstrap function was used for error estimation.

2.8 Bootstrapping

Bootstrapping is a resampling method calculating accuracy of sample estimates. This technique can be used on almost any statistic. An example of a property of an estimator that can be approximated by bootstrapping is the variance. The simple bootstrap technique uses the original data set of N members. A new sample is made (using for example MATLAB) that also has N members. The new sample is derived from the original sample using sampling with replacement[5], which means that it is not identical with the original sample. This is repeated some times, maybe 100 or 10 000 times, and for each of these bootstrap samples the mean or variance, for example, can be calculated (Diaconis & Efron 1983).

2.9 Estimating the cluster mass function

The estimation of the mass function is done in several steps. The cluster chosen to be analyzed is from the article by Wang et al. (2012), see section 2.10.3. Initially the 800 000 galaxies from the SDSS DR7 catalog (see section 2.10) are checked through and seen whether they satisfy a velocity and a distance constraint (see section 3.2.1). The velocity constraint is fixed, but the distance constraint, i.e. the size of the cluster, is varied. All the galaxies that meet these two requirements go through to the next step where an interloper removal method is applied (see section 3.2). Here galaxies not belonging to the cluster according to the interloper removal method are removed. The galaxy cluster mass as solar masses is now calculated using the virial mass estimator and the 200 overdensity mass, see section 2.2.1 and 2.6. In other words, the following relation must be satisfied:

$$\frac{M_{\mathrm{v}}}{\frac{4\pi}{3}\rho_{\mathrm{crit}}R_{\Delta}^{3}} = \Delta = 200 \tag{21}$$

That is, the virial mass calculated for the size of the cluster that corresponds best to the overdensity 200 is chosen as the cluster mass. These steps are repeated for all 200 clusters from Wang et al. (2012). The base ten logarithm of the cluster masses is taken and rounded to two decimal places. The next step is to divide the cluster mass data into ten bins. Now the mass function can be plotted: the number of clusters in each bin as a function of the bin masses. The data points for the largest masses are often very scattered and therefore cut off.

[5] Sampling with replacement is when a unit selected at random from the population is returned to the population, and then a second element is selected at random, and so on.

2.10 Data

Three data sets were used: The Sloan Digital Sky Survey (SDSS) Data Release 7 (DR7) catalog, the Gaussian Mixture Brightest Cluster Galaxy (GMBCG) catalog and around 200 clusters from Wang et al. (2012). The SDSS DR7 catalog was used for galaxy data, the GMBCG for the cluster data and Wang et al. (2012) for having a set of clusters with mass data for X-ray clusters to compare to. For all data sets right ascension, declination and redshift (z) was used.

2.10.1 SDSS

The SDSS DR7 catalog is used to provide redshift, right ascension and declination of around 800 000 galaxies. The SDSS is a spectroscopic redshift and major multi-filter imaging redshift survey. Projects involving mapping the sky have been carried out since the year 2000, and more will be realized in the near future. Since the beginning of the data collection, over 35% of the sky has been mapped.

The SDSS DR7 includes 11 663 deg^2 imaging data and contains five-band photometry for 357 million distinct objects[6]. The spectra includes 930 000 galaxies, 120 000 quasars and 460 000 stars (Abazajian et al. 2009).

2.10.2 GMBCG

The GMBCG cluster catalog for SDSS DR7 covers the legacy survey area of SDSS[7]. It has redshifts in the range of $z \in [0.1,0.55]$ and consists of over 55 000 rich clusters. The algorithm for detecting clusters is based on identifying the red sequence[8] and Brightest Cluster Galaxy (BCG) feature. The red sequence is found by the use of Error Corrected Gaussian Mixture Model (Hao et al. 2010). The BCG and red sequence pattern is a unique feature of galaxy clusters, and thus the identification of this feature is an important step in the cluster finding algorithm. The distribution of galaxy colours can be approximated as one redder and narrower Gaussian distribution which corresponds to the cluster's red sequence, and one bluer and wider Gaussian distribution which corresponds to foreground and background galaxies and the blue cluster members. In figure 1 the galaxy colour distribution around a cluster can be seen. If there is no cluster in the sky, there will be only one wide Gaussian that represents the colour distribution in a part of the sky. Isolating the red sequence galaxies, the problem of finding clusters reduces to an analysis of clusters in

[6]In the five-band photometry, the aperture in all bands is set by the profile of the galaxy in the R band alone. This procedure ensures that the colour measured by comparing the Petrosian flux F_p in different bands is measured through a consistent aperture. The Petrosian flux in any band is defined as the total flux within a radius of $2r_\mathrm{p}$: $F_\mathrm{p} = \int_0^{2r_\mathrm{p}} 2\pi r I(r)\,\mathrm{d}r$, where $I(r)$ is the azimuthally averaged surface-brightness profile and the Petrosian radius, r_p, is the radius at which the local surface-brightness average in $0.8r_\mathrm{p} - 1.25r_\mathrm{p}$ is 20% of the mean surface-brightness within r_p (Deng et al. 2007).

[7]The Sloan Legacy Survey which was a part of the SDSS-II project in between year 2005 and 2008, covers over 7 500 squares degrees of the Northern Galactic Gap with spectra from over 800 000 galaxies and 100 000 quasars (Hao et al. 2010)

[8]The red sequence includes most red galaxies which are generally elliptical galaxies.

the RA and Dec plane. The next step will then be to either use parametric or non-parametric methods to analyze the cluster signal strength.

When searching for clusters across a broad redshift range there is an increasing risk of finding overlapping clusters. This will give a different colour distribution and will complicate the selection process. The application of a broad photometric redshift[9] window for cutting off galaxies before searching the colour distribution, reduces the possibility of overlapping clusters to occur.

Another complication is that the red sequence galaxies selected from different colour band have different degrees of contamination from the background. Thus once a cluster catalog is produced, further calibration of the richness measured from different colour bands is needed, using another analysis such as gravitational lensing.

The GMBCG uses the BCG's as cluster centers. The main motivation for this is that the brightest galaxy in a cluster often is the central galaxy in a cluster.

More information about the cluster selection can be found in Hao et al. (2010).

2.10.3 200 clusters from Wang et al. (2012)

In Wang et al. (2012) a sample of around 200 cross-identified X-ray clusters and their approximated group halo masses are given. Initially Wang et al. (2012) made an eyeball check of the central galaxies that were linked with X-ray clusters in the SDSS DR7 sky coverage. And further the optical groups were linked with the X-ray clusters according to their central galaxies. Then Wang et al. (2012) checked the general correlation between the optical and X-ray properties for all the X-ray clusters, and found that the stellar mass of the central galaxy was correlated with the X-ray luminosity. When comparing two sets of halo masses for the X-ray clusters, Wang et al. (2012) found that the cluster mass $M_{\rm X}$ estimated from their X-ray luminosity were in general agreement with the group mass estimated from the stellar mass, $M_{\rm G}$.

[9]The photometric redshift is an estimate for the distance of an astronomical object. The technique uses photometry (i.e. the brightness of the object viewed through various standard filters, each of which lets through a relatively broad spectrum of colours) to determine the redshift and thus the distance to the observed object (Bolzonella et al. 2000).

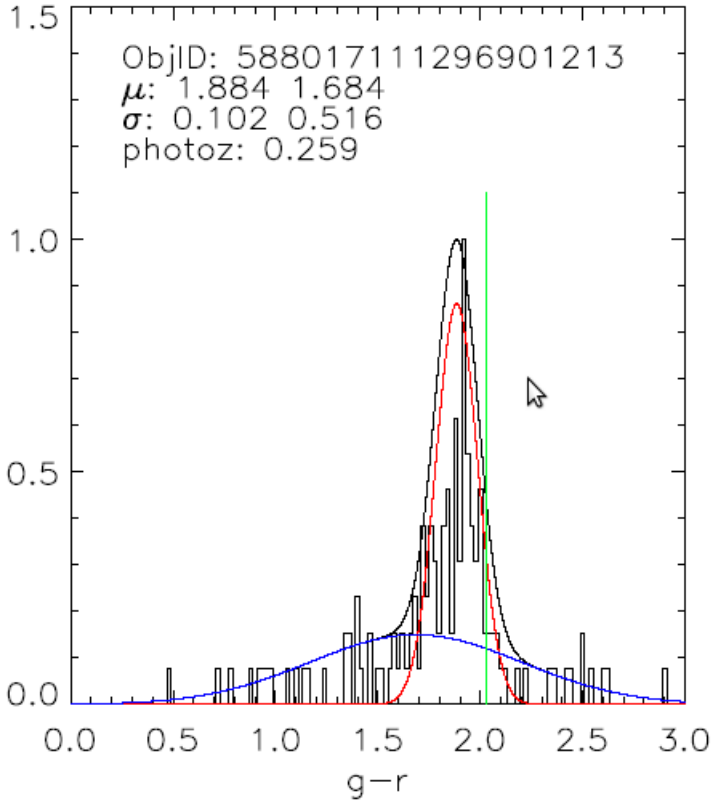

Figure 1: The colour distribution around a representative cluster overlaid with a model constructed of a mixture of two Gaussian distributions. The red curve is the red sequence component, the blue curve is the sum of background galaxies and blue cluster members, and the green vertical line indicates the colour of the BCG. The μ and the σ component are mean and the standard deviation of the two Gaussian components (Hao et al. 2010).

3 Analysis

Different methods and ways of approaching the problem of estimating cluster masses and finding a mass function have been used. Section 3.1 explains how the problems was initially approached and the progress that followed. Section 3.2 describes the methods used for finding cluster members.

3.1 Procedure

The procedure is described with the following steps:

1. The initial step in the process was to use a single cluster, in this case the Abell cluster A119[10], and to this apply a simple interloper removal method, **the 2-3σ-clipping approach** (see section 3.2.3). A first step in all of the interloper removal methods was to set a maximum velocity for every galaxy with respect to the cluster center, as well as a maximum distance to the cluster center. Setting the initial velocity condition to less than |4000| km/s and the maximum distance to the cluster center to 2 Mpc, a group of 149 cluster members was singled out. After these initial constraints, the 3σ-clipping approach was implemented - however when using the rough value three times the standard deviation, 3σ, no galaxies were removed as interlopers. Looking at the distribution of the 149 cluster members (velocity versus distance from cluster center) it would seem that the 3σ approach would not sort out some galaxies that by the look of it should not belong to the cluster. However, when using a 2.5σ-cut, some of the outlying galaxies were removed. Figure 9 shows how the 2-3σ-clipping approach removes galaxies from the cluster. Both 2.5σ and 3σ approaches gave an overestimation of the virial mass compared to data from Horner et al. (1999) and Rines et al. (2003). The same procedure was made for 14 other clusters: A1885, A0085, A0295, A0671, A0957, A1066, A1205, A1424, A1552, A1750, A2061, A2175, A2255, A2670. Even for these clusters the masses were overestimated.

2. The second step was to use clusters A119 and A1885, using the same initial velocity and distance constraints as before, but now applying **the maximum velocity approach** on the clusters, see section 3.2.2. This interloper removal method seemed to remove many more outlying galaxies than before.

3. In the third step, the clusters A119 and A1885 were used once again, but now applying another interloper removal method, **the virial mass projected mass ratio approach** (see section 3.2.5). It was easier to determine how many interlopers there was in A119 than in A1885 by the use of this method. Comparing the results for A119 from the virial mass projected mass ratio approach to the maximum velocity approach, it seemed they agreed well. However the virial mass projected mass ratio approach was much more time consuming and could not be automatized as the previous interloper removal methods could.

[10]The data on clusters A119, A1885, A0085, A0295, A0671, A0957, A1066, A1205, A1424, A1552, A1750, A2061, A2175, A2255, A2670 are from the GMBCG catalog (see section 2.10.2).

So this method was decided to be used only as verification for the maximum velocity approach.

4. In the fourth step, the maximum velocity approach was modified to calculate the **200 overdensity masses** (see equation 19) for the set of 15 clusters previously mentioned. This made it easier to compare the cluster masses with already existing data from articles such as Horner et al. (1999). The initial velocity constraint was varied between 1500 km/s to 5000 km/s.

5. In the fifth step the cluster data was expanded to **the 200 clusters from Wang et al. (2012)**. The masses were calculated using the 2-3σ-clipping approach and the maximum velocity approach, and compared with the data in Wang et al. (2012). Examining the data it was seen that binary clusters (see figure 2) were overestimating the cluster masses. Thus a method to remove one of the two parts in the binary cluster was implemented: **the polyfit method approach** (see paragraph 3.2.2). A modified initial velocity criteria was also tested, see equation (22) in section 3.2.1.

6. In the sixth step another interloper removal method was introduced, **the maximum velocity gap approach** (see section 3.2.4) and applied on the 200 cluster sample. The initial velocity constraint was set to 4000 km/s and the velocity gap was varied between 70 km/s, 400 km/s, 500 km/s and 700 km/s.

7. In the seventh step **the mass function from Klypin et al. (2011)** was introduced. The reason for choosing this mass function to compare the data with was mainly because it was very hard finding articles giving an analytic expression of the mass function, and the mass function from Klypin et al. (2011) was in good agreement with results in Tinker et al. (2008) who present the evolution of the mass function for $z = 0$ to $z = -2.5$ for halos defined using the spherical overdensity. The explanation for how the cluster mass function is estimated is given in section 2.9. The cluster mass data from the different interloper removal methods was put into the mass function formula in equation (5). It was plotted in the same figure as the number of clusters versus cluster mass for the different interloper removal methods. The polynomial fitting method from MATLAB and the bootstrap method for finding error bars (see section 2.8) were applied on both mass functions, see figure 6.

8. The last step was to calculate **the quality of fit of the different interloper removal methods** taking error bars, residuals in the horizontal axis as well as the slope of the mass functions into account.

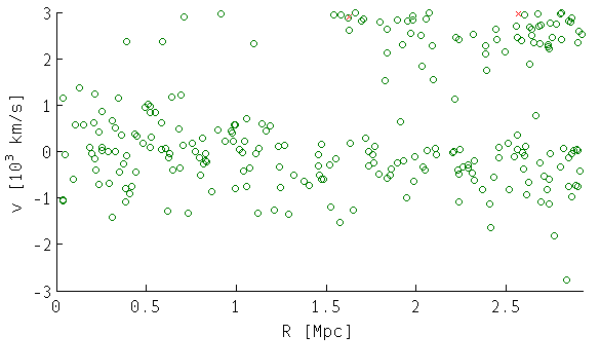

Figure 2: An example of a binary cluster. Velocity versus the radius with respect to the cluster core is plotted for all of the member galaxies.

3.2 Interloper Removal Methods

Explanations of the initial velocity constraint, distance constraint and the four different interloper removal methods that were used for the determination of cluster members are given below.

3.2.1 The Initial Velocity Constraints and Distance Constraints

Initially the velocity constraint for the cluster members was set to less than |4000| km/s with respect to the cluster center. As this constraint corresponds to at least 4σ in general for cluster objects, it would not cut off galaxies with high peculiar velocities. This constraint was further modified to |1500|, |2000|, |2500|, |3000|, |5000| km/s to see the effect of the mass when dealing with different interloper removal methods. The velocity cut |4000| km/s might not in every case cut away as many cluster members needed (depending on the interloper removal method). Another similar way to constrain the velocity of the cluster members that was used in the maximum velocity approach is:

$$c \cdot |z_{\text{cluster}} - z_{\text{galaxy}}| < 2000 \text{ km/s} \tag{22}$$

Before calculating the 200 overdensity mass (step 1-3 in section 3.1), the initial distance constraint for each cluster member to the cluster center was set to 2 Mpc.

3.2.2 The Maximum Velocity Approach

The maximum velocity approach sets a constraint on the cluster members infall and circular velocities. As we only know the projected distance relative to the cluster center of each galaxy, the galaxies can be anywhere on a vertical line at that projected distance within a circle of a certain radius R_{cluster}, see figure 3. The circular and infall velocity is given by:

$$v_{\text{circular}} = \sqrt{\frac{GM(r)}{r}} \tag{23}$$

$$v_{\text{infall}} = \sqrt{2} v_{\text{circular}} \tag{24}$$

where r is the distance to the galaxy and $M(r)$ is the virial mass from equation (3) of the cluster at that specific distance. To retrieve v_{circular} one must assume circular orbits of a given set of particles. The virial theorem can then be applied and the $U_{\text{circular}} = -2T_{\text{circular}}$ relation can be used. The infall velocity is defined as $T_{\text{infall}} = -U$, the upper limit to the velocities of the particles for which the virial theorem holds[11]. The maximum possible velocity along the line of sight from the cluster center is then given by (Wojtak et al. 2008):

$$v_{\text{max}} = \max\{v_{\text{infall}} \cos\theta, v_{\text{circular}} \sin\theta\} \tag{25}$$

where θ is the angle between the position vector of the particle with respect to the cluster center and the line of sight. In figure 3 an explanation of the method is shown. The black dots are galaxies and the orange dot is the cluster center. The total radii of the cluster is $\mathrm{R}_{\text{cluster}}$. In the maximum velocity approach the vertical line starting at $\mathrm{R}_{\text{projected}}$ ending at $\mathrm{R}_{\text{cluster}}$ is divided into small steps. In each of these steps, the circular and infall velocities are calculated. The maximum velocity a galaxy can have will then be the maximum of all the infall and circular velocities calculated in each step at that line. Thus the galaxies with peculiar velocities higher than v_{max} are cut off. However there is one problem that needs to be dealt with: the virial mass estimator does not consider the galaxy nearest to the cluster center. So there are three ways to approach this problem: not taking the galaxy nearest to the cluster center into account, taking it into account by saying that it has the same mass as the one right next to it, or taking it into account by investigating if any of the removed galaxies have smaller absolute velocities than the galaxy nearest to the core. If that is the case, the nearest galaxy is removed.

[11] The limit comes from the requirement that a particle in a given set is bound to the halo, i.e. $U + T < 0$

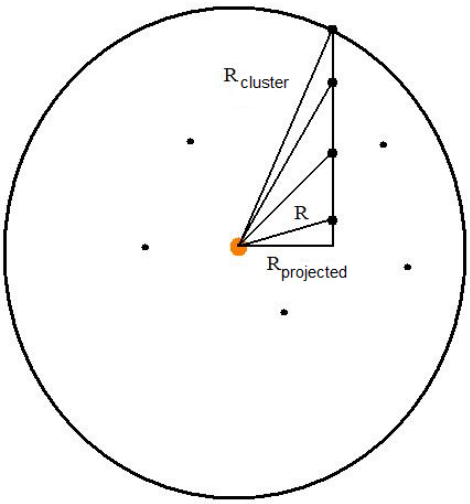

Figure 3: The black dots are galaxies and the orange dot is the cluster center. The total radii of the cluster is $R_{cluster}$. In the maximum velocity approach the vertical line starting at $R_{projected}$ ending at $R_{cluster}$ is divided into small steps. In each of these steps, the circular and infall velocities are calculated. The maximum velocity a galaxy can have will then be the maximum of all the infall and circular velocities calculated in each step at that line. Thus galaxies having a velocity greater than this maximum velocity is considered interlopers and removed from the cluster. This is repeated for all galaxies until the method converges.

Polyfit Method Approach A modified version of the maximum velocity approach is the 'polyfit method approach'. One step is added here: a method to remove binary clusters. Binary clusters, systems that have two distinct cumulated parts in the velocity versus distance plot for the cluster members (see figure 2), are always overestimated in mass. What the polyfit method approach does is that it checks if the cluster is a binary cluster, then it removes the less cumulated part of the binary system. The initial velocity constraint is set to 4000 km/s.

3.2.3 The 2-3σ-clipping Approach

In the 2-3σ-clipping approach the galaxies left after the initial velocity constraint of 4000 km/s is sorted after increasing velocities. The set of galaxies is then divided into 10 bins. The number of bins is just an arbitrary value. It then calculates the velocity dispersion of each bin and removes all galaxies with velocities larger than the mean of the bin ± 2-3σ. This is repeated until the method converges.

3.2.4 The Maximum Velocity Gap Approach

The maximum velocity gap approach sets a constraint to the absolute velocity difference between every pair of cluster members. The n cluster members (G_1,...G_n) that are filtered through the initial constraints in section 3.2.1 are sorted starting with the smallest velocity ending with the

largest in an array $S = [G_1,G_2,...,G_{median},G_{median+1},...,G_n]$. From here on S is divided into two subsets of galaxies, S_1 and S_2: from the first galaxy to the galaxy at the median velocity ($S_1 = [G_1,...,G_{median}]$), and from the galaxy right next to the galaxy at the median velocity to the galaxy with the largest velocity ($S_2 = [G_{median+1},...,G_n]$). The absolute velocity difference between every par in each of the two sets S_1 and S_2 are now calculated and put in two new arrays $S_{V,1}$ and $S_{V,2}$: $S_{V,1} = [|V_{G_1} - V_{G_2}|, |V_{G_2} - V_{G_3}|,...,|V_{G_{median-1}} - V_{G_{median}}|]$ and $S_{V,2} = [|V_{G_{median}} - V_{G_{median+1}}|, |V_{G_{median+1}} - V_{G_{median+2}}|,...,|V_{G_{n-1}} - V_{G_n}|]$. If any of the absolute velocity differences in $S_{V,1}$ are larger than the velocity gap chosen, for example 500 km/s, then the galaxy with the smallest velocity will be rejected, i.e. for $|V_{G_1} - V_{G_2}|$, G_1 will be considered an interloper. Further if any of the absolute velocity differences in $S_{V,2}$ are larger than the velocity gap chosen, then the galaxy with the largest velocity will be rejected (i.e. for $|V_{G_{n-1}} - V_{G_n}|$, G_n will be considered an interloper). This procedure is repeated until the method converges.

3.2.5 The Virial Mass Projected Mass Ratio Approach

This interloper removal method is dependent on the fact that the projected mass is highly affected by interlopers and the virial mass is not (Perea et al. 1990). After applying the initial constraints on the cluster (see section 3.2.1) there are n galaxies left. Two arrays, A1 and A2, are computed with the length n holding virial masses and projected masses. In the i:th position in the arrays are the virial mass and projected mass calculated by taking all n galaxies into account except for the i:th galaxy. The two masses in these arrays that contribute to the largest dispersion of A1 and A2, respectively, are removed from the cluster. This process is repeated until all galaxies are removed. The projected mass and virial mass are then plotted against the number of interlopers. The derivatives of the two mass estimators versus the number of interlopers are also plotted against the number of interlopers. The ratio between M_{p} and M_{v} is then investigated by eye to determine at what number of interlopers the two masses seem to converge (see figure 14). This approach is harder to automatize as one need to go in manually in several places. It is more time consuming than any of the other methods, and even if it was not used as a main method in this thesis, it was used as a validation for the maximum velocity approach method.

4 Results

Results from the derivation of the mass function on the 200 clusters from Wang et al. (2012) using the different interloper removal methods, and a comparison with Wang et al. (2012), are given in this section.

4.1 Mass function

The mass functions derived from the different interloper removal methods are approximated by the MATLAB polyfit method to the second degree:

$$a_1 \cdot \log_{10}(M/M_{\text{sun}})^2 + a_2 \cdot \log_{10}(M/M_{\text{sun}}) + a_3 \tag{26}$$

where a_{1-3} are polynomial constants and M is the 200 overdensity mass of the clusters. The error bars are σ scatter obtained from 10 000 bootstrap re-samplings.

The quality of fit of the different interloper removal methods is calculated from three procedures: the first sum up the horizontal residuals between the mass functions derived from the different interloper removal methods and the mass function from Klypin et al. (2011) in section 2.3:

$$\mathrm{p_1} = \sum_i \left(\log_{10}(M/M_{\text{sun}})_{\mathrm{K},i} - \log_{10}(M/M_{\text{sun}})_{\mathrm{IRM},i} \right) \tag{27}$$

The indices K and IRM stands for Klypin et al. (2011) and interloper removal method, respectively. The second procedure, $\mathrm{p_2}$, considers the slopes of the two mass functions:

$$\mathrm{p_2} = \frac{\max(\mathrm{a_{1,IRM}},\mathrm{a_{1,K}})}{\min(\mathrm{a_{1,IRM}},\mathrm{a_{1,K}})} + \frac{\max(\mathrm{a_{2,IRM}},\mathrm{a_{2,K}})}{\min(\mathrm{a_{2,IRM}},\mathrm{a_{2,K}})} \tag{28}$$

where $a_{\mathrm{n,IRM}}$ and $a_{\mathrm{n,K}}$ ($\mathrm{n} = 1,2$) are the polynomial constants in equation (26) for the mass function derived from the interloper removal methods and the mass function from Klypin et al. (2011). The third and last procedure, $\mathrm{p_3}$, calculates how well the slopes for the two functions agree by taking the errors into account:

$$\begin{aligned} \mathrm{p_3} = \min(\mathrm{a_{1,max,IRM}} - \mathrm{a_{1,min,K}}, \mathrm{a_{1,max,IRM}} - \mathrm{a_{1,max,K}}) + \\ \min(a_{1,\mathrm{min,IRM}} - a_{1,\mathrm{min,K}}, a_{1,\mathrm{min,IRM}} - a_{1,\mathrm{max,K}}) + \\ \min(a_{2,\mathrm{max,IRM}} - a_{2,\mathrm{min,K}}, a_{2,\mathrm{max,IRM}} - a_{2,\mathrm{max,K}}) + \\ \min(a_{2,\mathrm{min,IRM}} - a_{2,\mathrm{min,K}}, a_{2,\mathrm{min,IRM}} - a_{2,\mathrm{max,K}}) \end{aligned} \tag{29}$$

where $a_{\mathrm{n_1,n_2,n_3}}$ ($\mathrm{n_1} = 1,2$, $\mathrm{n_2} = \min, \max$, $\mathrm{n_3} = \mathrm{IRM, K}$) represent the polynomial constants in equation (26) as before but now taking the errors into account. Thus $a_1 \pm$ error and $a_2 \pm$ error will have a maximum and a minimum value. If the $a_{1,\mathrm{IRM}} \pm$ error lies within $a_{1,\mathrm{K}} \pm$ error, then the quality of the fit is zero.

The mass functions derived from the different interloper removal methods are projected down in the vertical direction with a factor corresponding to where the sum of the vertical residuals between the mass function from the interloper removal methods and the mass function from

Klypin et al. (2011) is the smallest. The constant factor a_3 in equation (26) is thus not taken into account when calculating the quality of fit of the two curves. The reason is because the unit of M dn/dM [h^3 Mpc^{-3}] could not directly be converted to the unit number of clusters. Thus the quality of fit is only calculated by the 'slope coefficients' a_1 and a_2.

In figures 6-8, 11, 12 and 13 the red curve with error bars corresponds to the mass function from Klypin et al. (2011) using the cluster masses derived from the different interloper removal methods, and the dark blue curve corresponds to a polynomial fitting to the second degree of the mass function data (the light blue points with error bars) derived from different interloper removal methods.

4.2 The Maximum Velocity Approach

How the method removes interlopers in each iteration for A0085 with initial velocity constraint of 4000 km/s can be seen in figure 4. Here the size of the cluster is $r = 3.84$ Mpc, and $M = 2.10 \cdot 10^{15} M_{\text{sun}}$. The plots of interloper removal for A2029 are displayed in figure 5. The data of the results are displayed in table 1 and the mass functions for this interloper removal method can be seen in figures 6, 7 and 8.

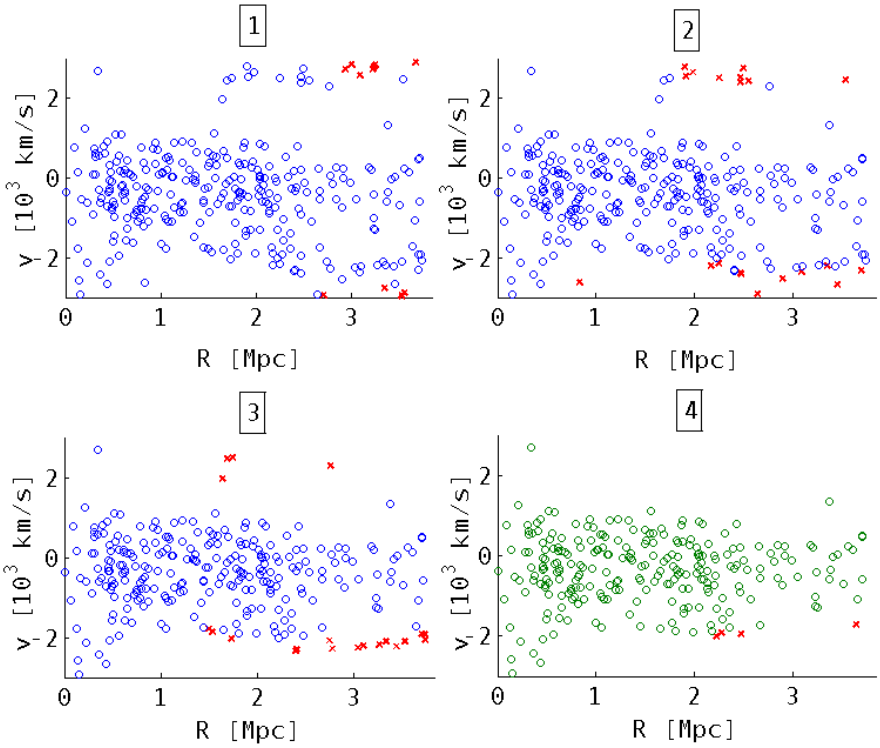

Figure 4: Cluster A0085 with initial velocity constraint 4000 km/s. The numbers 1-4 represent iterations. The green or blue rings represent cluster members, and the red crosses are interlopers removed using the maximum velocity approach in section 3.2.2. The plot with the green rings is the plot where the method has converged and stabilized.

4.3 The 2-3σ-clipping Approach

In figure 9 it can be seen how the different σ-cuts changes the number of cluster members. The 3σ-cut would not remove any interlopers after the cut off in section 3.2.1 for A119. Figure 10 shows the velocity distribution, which is fairly gaussian as expected, for the cluster members in A119 after a 2.5σ-cut. As the virial mass for A119 after the initial cut, $1.39 \cdot 10^{15} M_{\text{sun}}$, seems to be overestimated according to Horner et al. (1999) and Rines et al. (2003), smaller σ-cuts are used. Using a 2σ-cut, the virial mass becomes smaller, $4.86 \cdot 10^{14} M_{\text{sun}}$. The results and mass function from this method can be seen in table 1 and in figure 11, respectively.

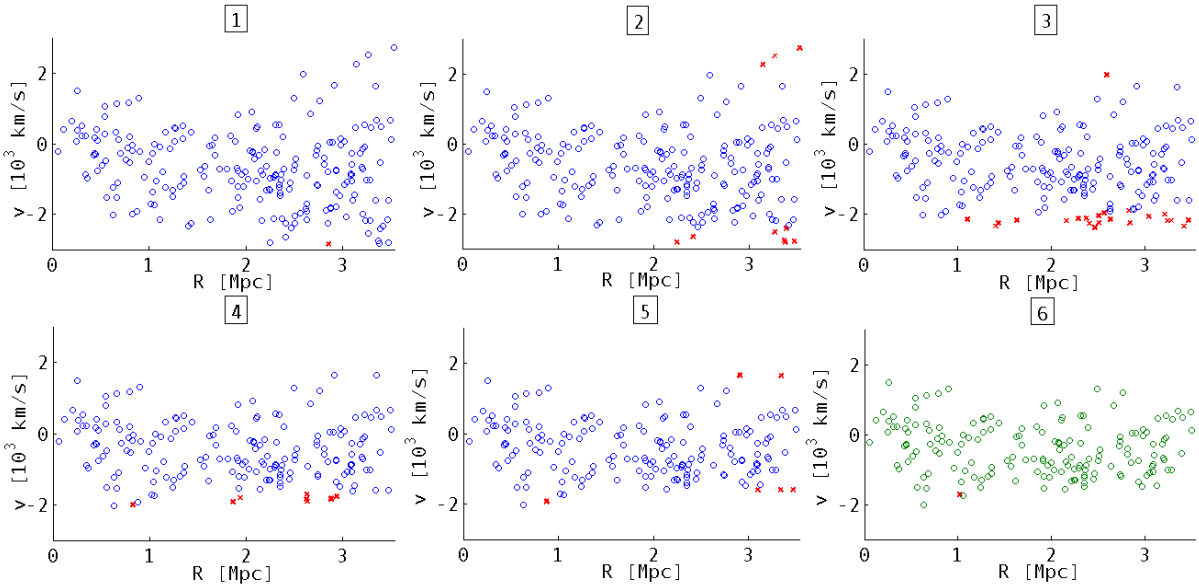

Figure 5: Cluster A2029 with initial velocity constraint 4000 km/s. The numbers 1-6 represent iterations. The green or blue rings represent cluster members, and the red crosses are interlopers removed using the maximum velocity approach in section 3.2.2. The plot with the green rings is the plot where the method has converged and stabilized.

4.4 The Maximum Velocity Gap Approach

The velocity gap between the galaxies was set to the values 70 km/s, 400 km/s, 500 km/s and 700 km/s. For each velocity gap, cluster members were selected and the mass function could be derived. The results are displayed in table 1 and the mass functions for this interloper removal method can be seen in figures 12 and 13.

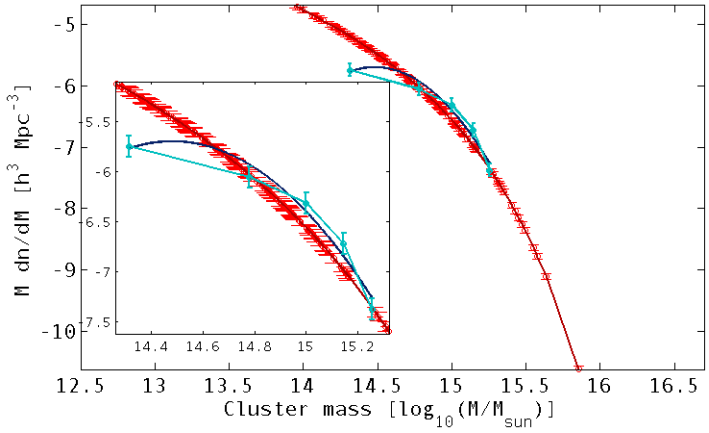

(a) Polyfit method with velocity constraint 4000 km/s

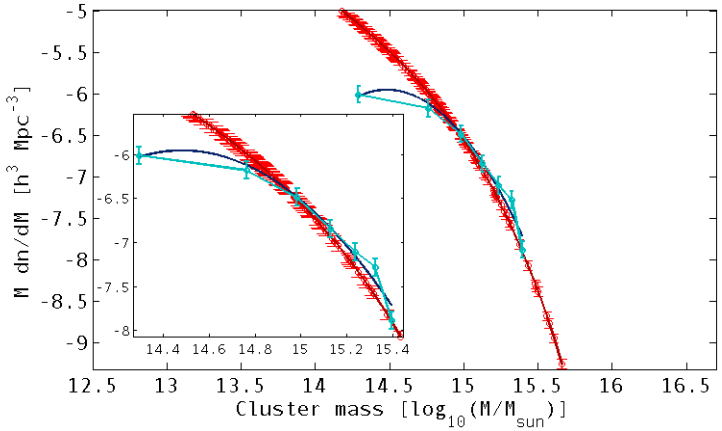

(b) Different velocity criteria method (see equation (22))

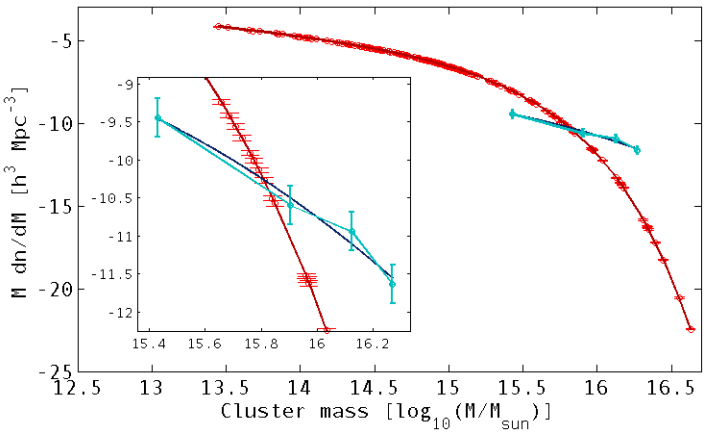

(c) Maximum velocity approach with velocity constraint 5000 km/s

Figure 6: The number of clusters versus cluster mass for different interloper removal methods. The red curve is the mass function from Klypin et al. (2011) with error bars. The darker blue curve is a polyfit of the mass function of the 200 clusters from Wang et al. (2012) derived from interloper removal methods, and the light blue curve is the same data however unfitted and with error bars. The smaller figure is a zoom in of the important part of the larger figure.

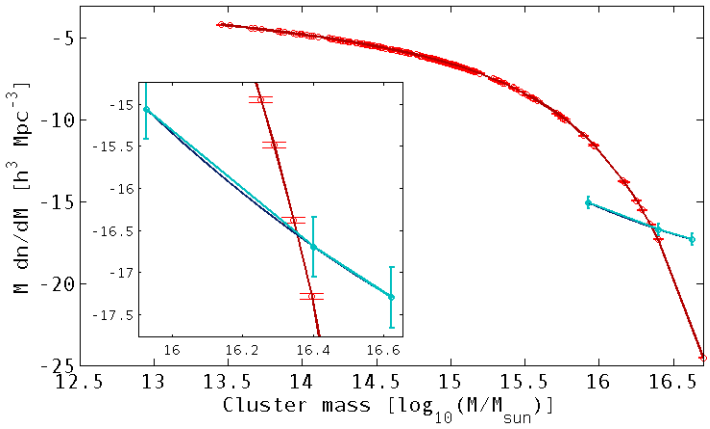

(a) Maximum velocity approach with velocity constraint 4000 km/s

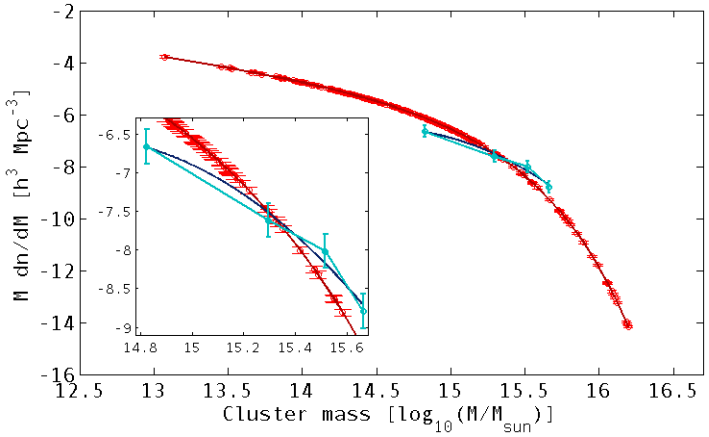

(b) Maximum velocity approach with velocity constraint 3000 km/s

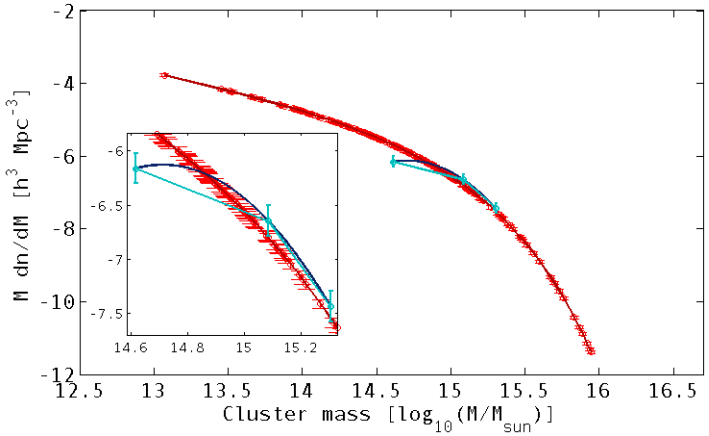

(c) Maximum velocity approach with velocity constraint 2500 km/s

Figure 7: The number of clusters versus cluster mass for different interloper removal methods. The red curve is the mass function from Klypin et al. (2011) with error bars. The darker blue curve is a polyfit of the mass function of the 200 clusters from Wang et al. (2012) derived from interloper removal methods, and the light blue curve is the same data however unfitted and with error bars. The smaller figure is a zoom in of the important part of the larger figure.

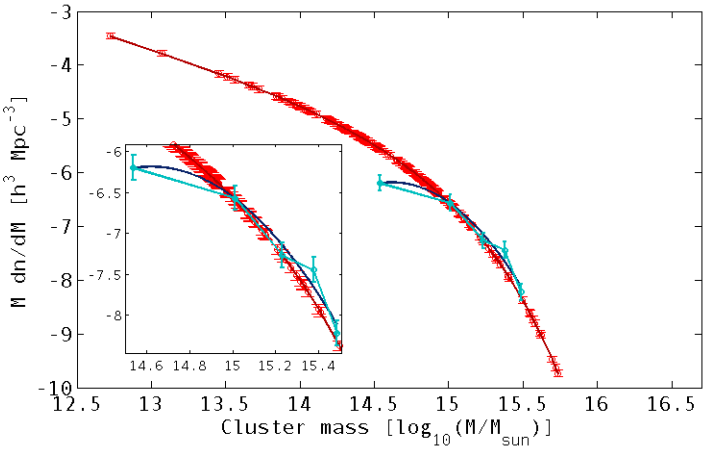

(a) Maximum velocity approach with velocity constraint 2000 km/s

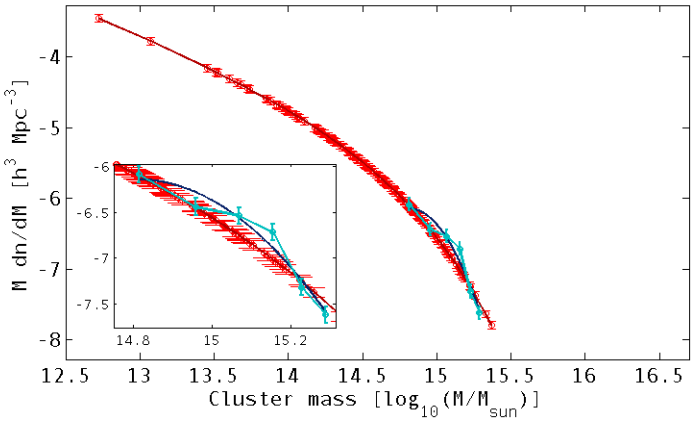

(b) Maximum velocity approach with velocity constraint 1500 km/s

Figure 8: The number of clusters versus cluster mass for different interloper removal methods. The red curve is the mass function from Klypin et al. (2011) with error bars. The darker blue curve is a polyfit of the mass function of the 200 clusters from Wang et al. (2012) derived from interloper removal methods, and the light blue curve is the same data however unfitted and with error bars. The smaller figure is a zoom in of the important part of the larger figure.

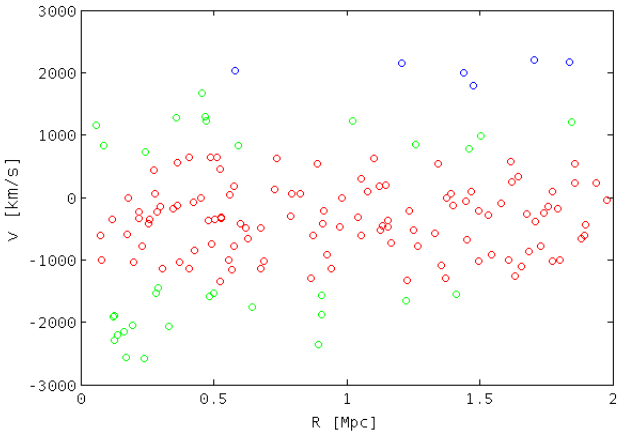

Figure 9: A plot of interlopers and cluster members for A119 using the 2-3σ-cut (see section 3.2.3). The blu
respectively.

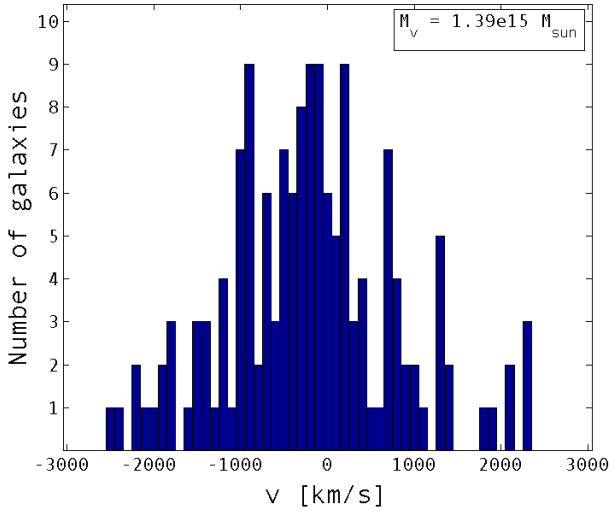

Figure 10: The velocity distribution for A119 using a 2.5σ-cut (see section 3.2.3).

4.5 The Virial Mass Projected Mass Ratio Approach

Figure 14a shows how the derivative of the two mass estimators with respect to the number of interlopers is converging and is approximately fully converged at 70 interlopers. This number of interlopers corresponds well to the number found by the maximum velocity approach. In figure 14b it can also be seen that the two masses converge. However in that plot it is more difficult to determine at what number of interlopers one should make the cut. Figures 15a and 15b show the same type of plots as before, for A1885.

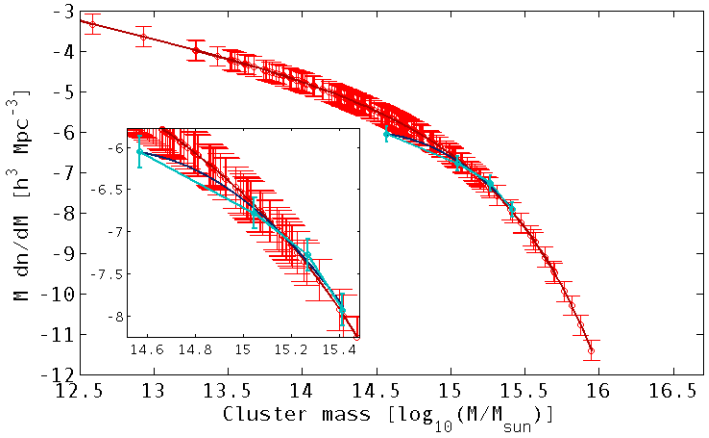

(a) 2σ-cut

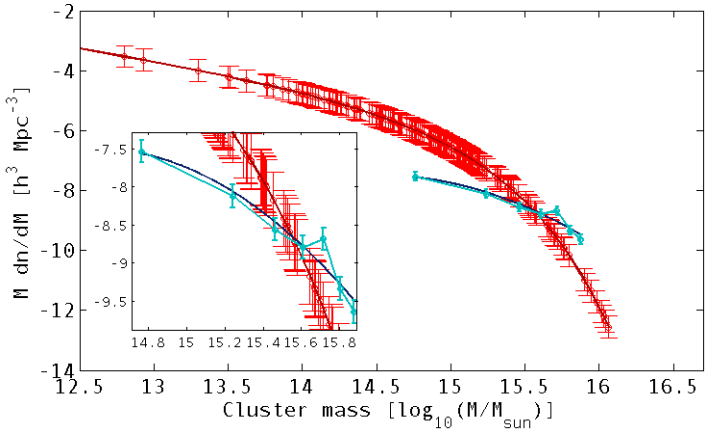

(b) 2.5σ-cut

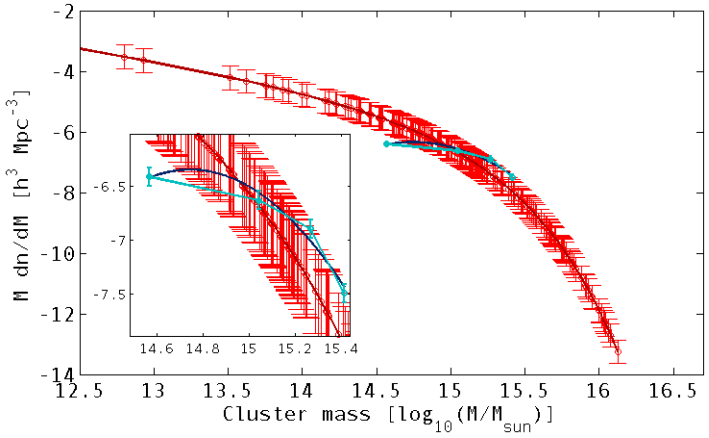

(c) 3σ-cut

Figure 11: The number of clusters versus cluster mass for different interloper removal methods. The red curve is the mass function from Klypin et al. (2011) with error bars. The darker blue curve is a polyfit of the mass function of the 200 clusters from Wang et al. (2012) derived from interloper removal methods, and the light blue curve is the same data however unfitted and with error bars. The smaller figure is a zoom in of the important part of the larger figure.

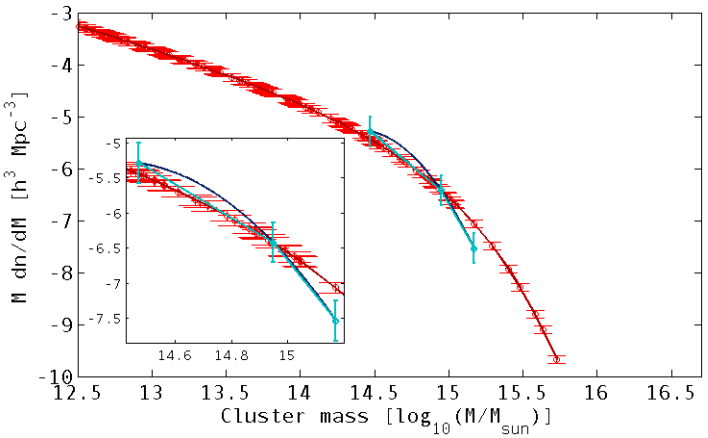

(a) A gap of 70 km/s

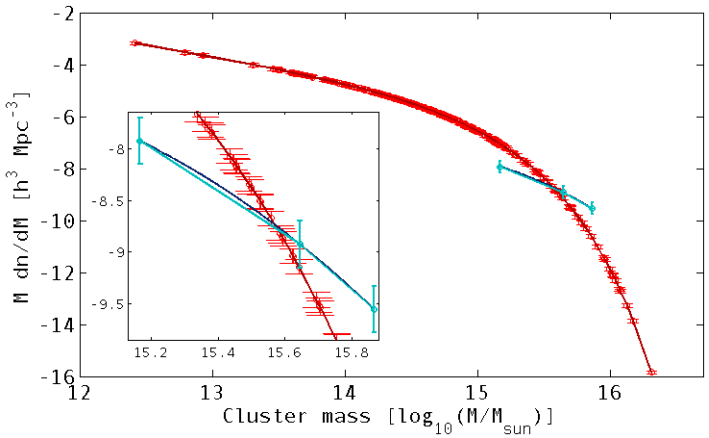

(b) A gap of 400 km/s

Figure 12: The number of clusters versus cluster mass for different interloper removal methods. The red curve is the mass function from Klypin et al. (2011) with error bars. The darker blue curve is a polyfit of the mass function of the 200 clusters from Wang et al. (2012) derived from interloper removal methods, and the light blue curve is the same data however unfitted and with error bars. The smaller figure is a zoom in of the important part of the larger figure.

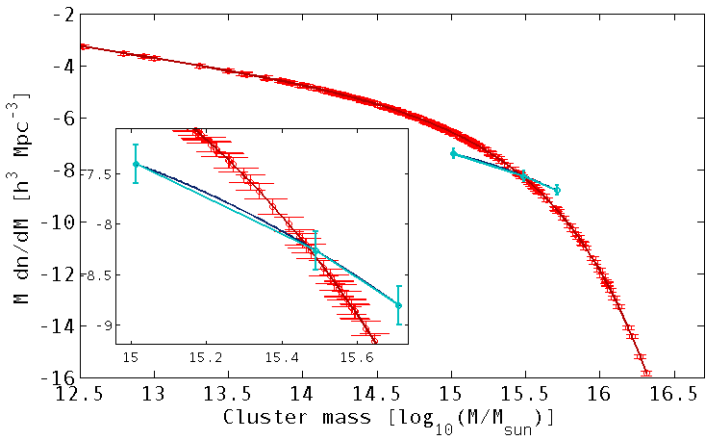

(a) A gap of 500 km/s

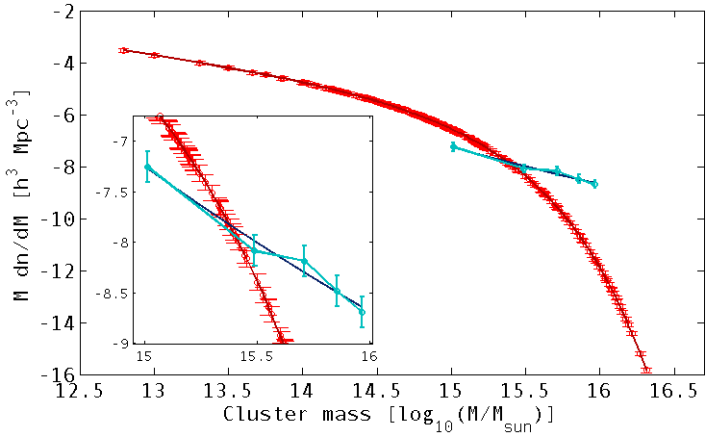

(b) A gap of 700 km/s

Figure 13: The number of clusters versus cluster mass for different interloper removal methods. The red curve is the mass function from Klypin et al. (2011) with error bars. The darker blue curve is a polyfit of the mass function of the 200 clusters from Wang et al. (2012) derived from interloper removal methods, and the light blue curve is the same data however unfitted and with error bars. The smaller figure is a zoom in of the important part of the larger figure.

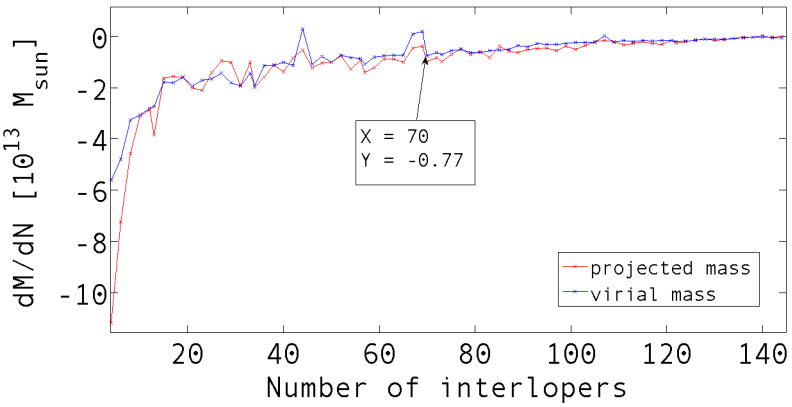

(a) The derivative of M_v and M_p versus the number of interlopers.

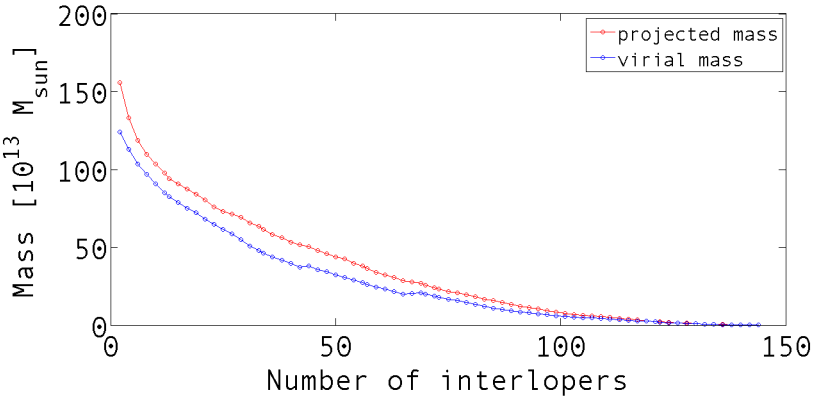

(b) M_v and M_p versus the number of interlopers.

Figure 14: The virial mass over projected mass method for cluster A119. The arrow in the upper figure points to the place where the two mass estimators are approximately fully converged.

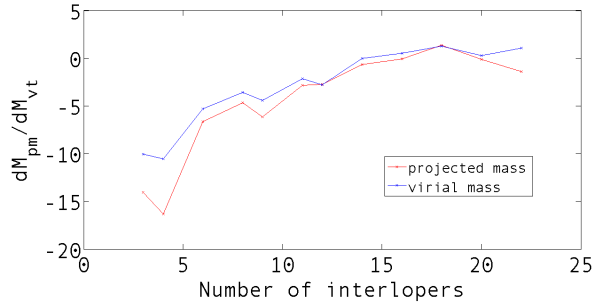

(a) The derivative of M_v and M_p versus the number of interlopers.

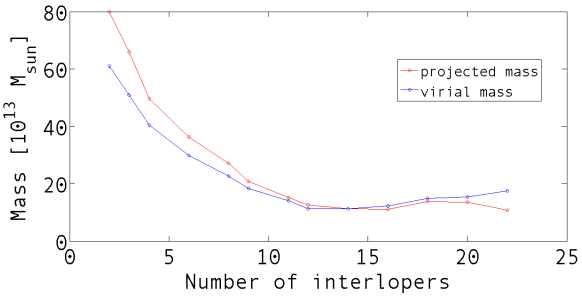

(b) M_v and M_p versus the number of interlopers.

Figure 15: The virial mass over projected mass method for cluster A1885.

Methods	p_1	p_2	p_3	Sum	Figure
Maximum Velocity Approach, 3000 km/s	0.380	0.220	0.094	0.69	7b
2σ-clipping Approach	0.280	0.311	0.422	1.01	11a
Maximum Velocity Approach, 1500 km/s	0.25	0.367	0.390	1.07	8b
Maximum Velocity Approach, 2000 km/s	0.43	0.399	0.800	1.63	8a
Maximum Velocity Gap Approach, 500 km/s	0.40	0.507	0.849	1.76	13a
Different Velocity Criteria, 2000 km/s	0.75	0.416	0.628	1.79	6b
3σ-clipping Approach	0.68	0.398	0.717	1.80	11c
Polyfit Method Approach	0.56	0.547	0.940	2.05	6a
Maximum Velocity Gap Approach, 400 km/s	0.40	0.551	1.130	2.08	12b
Maximum Velocity Approach, 2500 km/s	0.30	0.596	1.520	2.42	7c
Maximum Velocity Gap Approach, 70 km/s	0.22	0.653	1.570	2.44	12a
2.5σ-clipping Approach	1.30	0.468	0.803	2.57	11b
Maximum Velocity Approach, 5000 km/s	0.74	0.314	2.690	3.74	6c
Maximum Velocity Approach, 4000 km/s	0.60	-0.228	5.530	6.36	7a
Maximum Velocity Gap Approach, 700 km/s	1.21	-1.662	13.740	16.60	13b

Table 1: Tabular over the different interloper removal methods and their values of quality of fit. p_1, p_2 and p_3 are described in section 4 and by equations (27), (28) and (29). The column of the sum is displaying the sum of the different p factors in decreasing order. The smallest number of the sum gives the best interloper removal method considering all the p factors. The last column gives the figures of the plots of the mass function for each interloper removal method.

4.6 Comparison with data from Wang et al.

A comparison with the cluster masses in Wang et al. (2012) and the masses derived from the different interloper removal methods was made. Four plots of $\log(M/M_{\text{sun}})$ with errors bars included for the masses derived from the different interloper removal methods and the masses in Wang et al. (2012) as well as a 1:1 line, can be seen in figure 16. The error bars are σ scatter obtained from 10 000 bootstrap re-samplings. Data above the realistic limit $10^{15} M_{\text{sun}}$ for cluster masses have been cut off. In table 2 are the vertical residuals for cluster mass data from Wang et al. (2012) versus cluster mass data from one of the interloper removal methods to a 1:1 line (see figure 16).

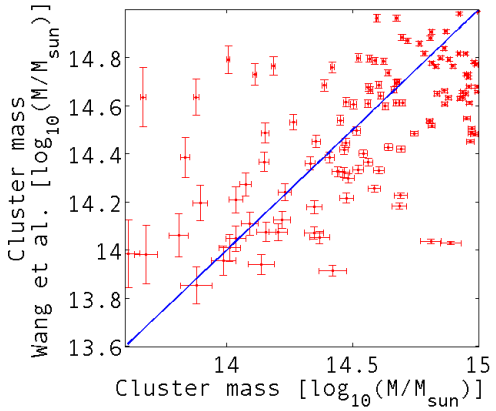

(a) The DVC2 interloper removal method.

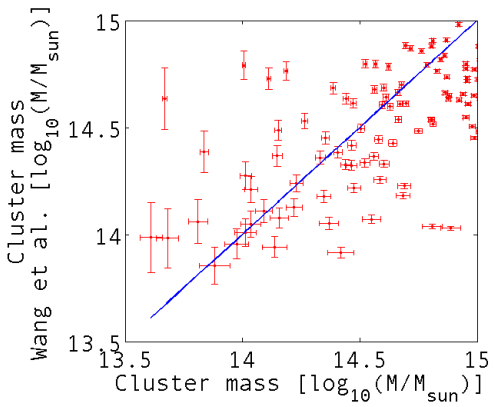

(b) The MVC3 interloper removal method.

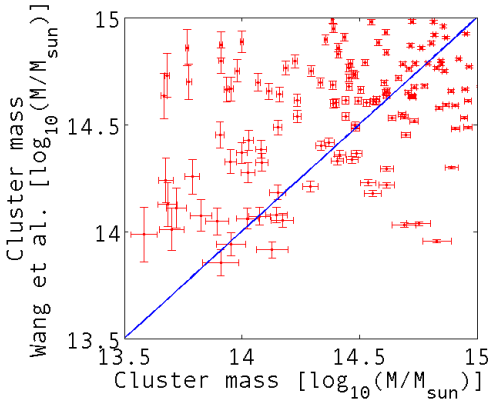

(c) The 2σ interloper removal method.

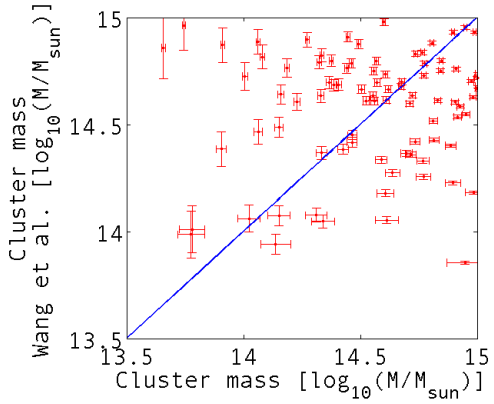

(d) The MVGM500 interloper removal method

Figure 16: The red dots with error bars are cluster mass data from Wang et al. (2012) versus cluster mass data from one of the interloper removal methods. The blue line is a 1:1 line for a better observation of the correspondence between the cluster masses. Data above $10^{15} M_{\text{sun}}$ have been cut off.

Methods	Residuals
3σ-clipping Approach	19
Maximum Velocity Approach, 5000 km/s	22
Maximum Velocity Gap Approach, 700 km/s	22
Maximum Velocity Approach, 4000 km/s	23
Maximum Velocity Approach, 3000 km/s	23
Maximum Velocity Approach, 2500 km/s	23
Maximum Velocity Approach, 2000 km/s	24
Different Velocity Criteria, 2000 km/s	26
2.5σ-clipping Approach	27
Maximum Velocity Approach, 1500 km/s	29
Maximum Velocity Gap Approach, 500 km/s	31
Polyfit Method Approach	32
Maximum Velocity Gap Approach, 400 km/s	41
2σ-clipping Approach	45
Maximum Velocity Gap Approach, 70 km/s	273

Table 2: The second column displays the vertical residuals for cluster mass data from Wang et al. (2012) versus cluster mass data from one of the interloper removal methods to a 1:1 line (see figure 16).

5 Discussion

The mass function of 200 clusters from Wang et al. (2012) has been derived using three interloper removal methods: the maximum velocity approach (MVA), the 2-3σ-clipping approach (2-3σ) and the maximum velocity gap approach (MVGA). The virial mass has been used for estimating the 200 overdensity cluster masses. The quality of fit, how well the mass function agrees with the mass function from Klypin et al. (2011), has been calculated taking the residuals in the horizontal axis with error bars and the slope of the mass function from the different interloper removal methods into account.

Discussion of the results are divided into the three sections Interloper removal methods, Cluster mass functions, Systematic errors and uncertainties and Ideas for the future.

5.1 Interloper removal methods

The MVA using a velocity constraint of 3000 km/s agrees best with the mass function derived analytically by Klypin et al. (2011). A 3000 km/s velocity cut means that galaxies in the cluster can at most have a velocity of 3000 km/s relative to the cluster center. Hubble's law gives a corresponding galaxy distance of approximately 40 Mpc. Thus the maximum radii of the cluster is 40 Mpc if only setting a constraint on the velocities of the galaxies. Superclusters with sizes up to 50 Mpc in radii exist, but are uncommon. Hence the 3000 km/s velocity constraint is physically relevant, even if it might exclude a supercluster (a standard velocity constraint is 4000 km/s, which give a radii of approximately 50 Mpc).

The 2σ also agrees well with the mass function from Klypin et al. (2011). However it is clear that when there is an excess of interlopers or too few member galaxies in the cluster, all three methods give a larger uncertainty and a systematically different slope of the mass function.

One reason for why the MVA in general seems to agree better with the mass function from Klypin et al. (2011), is that MVA takes both the distance from the cluster center and velocity for each galaxy into consideration when choosing the cluster members. The 2-3σ and the MVGA do only consider the velocities of the galaxies when determining the cluster members. As mentioned, for the MVA the 3000 km/s velocity constraint gives the best result. As a 3000 km/s velocity constraint is in between 1500 km/s and 5000 km/s, it could be deduced that the 3000 km/s velocity constraint does not take too many or too few member galaxies into account. A harsh velocity constraint (such as 1500 km/s) may cut off an excessive amount of galaxies which gives a smaller cluster mass approximation than it should. But it seems that not removing enough interlopers makes even a less accurate mass estimate than when removing too many. The same analysis can be done on the MVGA, where a velocity gap of 500 km/s gives the best result. However, the 2σ gives the best result for the 2-3σ-clipping approach, i.e. the σ method cutting off most galaxies.

Mamon et al. (2010) mentions that the 2.7σ method can only distinguish the quarter of galaxies that are interlopers from those satisfying the virial theorem criteria (see section 2.1). The 3σ will thus probably give a result too contaminated by interlopers to trust. However, as the 2σ has a much harsher velocity constraint it obviously cuts off more interlopers and thus give a more reliable result. According to Wojtak et al. (2008) the MVA leads to the data sample which re-

produces real velocity dispersion better than the one obtained after applying the 3σ. One can thus deduce that their MVA gives a better estimate of the mass function than the 3σ does, which confirms the results in this thesis that MVA in general gives a better correspondence to the mass function from Klypin et al. (2011).

5.2 Cluster mass functions

The mass function from Klypin et al. (2011) is derived using quite complicated analytical expressions. However it is clearly stated in the article that the mass function approximation has an accuracy of more than 2% for masses $M > 10^7 h^{-1} M_{\text{sun}}$. Moreover the mass function from Klypin et al. (2011) is in good agreement with results in Tinker et al. (2008), who present the evolution of the mass function for $z = 0$ to $z = -2.5$ for halos defined by using the spherical overdensity. The mass function from Klypin et al. (2011) is thus reliable and good for mass function comparison.

Looking at figures 6-8, 11, 12 and 13, there seems in general to be too few clusters with masses less than $10^{15} M_{\text{sun}}$. This effect could be due to the few number of clusters used, or because some of the interloper removal methods does not remove enough galaxies in each cluster, thus making the cluster more massive.

5.3 Systematic errors and uncertainties

There are mainly three factors that induce systematic errors when estimating the mass function: the mass estimator, the interloper removal method and the set of clusters that is examined.

The virial mass estimator requires a system that is in equilibrium, and because it is hard to establish if the clusters are merging, approximately spherically symmetric or are in some other way not in equilibrium, it is not straight forward if the virial mass estimator should be applied on every cluster in the set of 200 clusters from Wang et al. (2012).

There are only 200 clusters in the set being analyzed which could of course be expanded for a better result and a larger mass interval. This would also make it easier to estimate the quality of fit of the interloper removal methods. The computer used for the programming was an Asus U46SV-WX011V with the processor model Intel Core i5. The time it took running the MVA on the 200 clusters was around 12 hours. Running the program on a set of 50 000 clusters would thus take 125 days. It would of course go much faster if it was run on a better computer than the one used for this thesis. However the run time indicates that the interloper removal methods are complicated and time consuming, and could probably be improved in many ways to reduce the run time.

Furthermore the masses in Wang et al. (2012) are calculated in a different way than in this thesis, and thus the comparison in figure 16 is only to be used as an affirmation that the two sets of masses approximately, with some scattering, lie on a 1:1 line when plotting them against each other. In general the clusters lie a bit above the 1:1 line. This systematic difference indicates that the clusters from Wang et al. (2012) are slightly more massive than the masses derived from the different interloper removal methods. It is hard to see where this systematic difference originates from as the masses in Wang et al. (2012) and the masses from the interloper removal

methods are derived differently. One suggestion is that the difference is due to the choices of the cosmological constants (σ_8 and/or Ω_m) used in Wang et al. (2012). Looking at table 2, the best fit of the interloper removal methods to the 1:1 line (see figure 16) does not coincide with the best result in table 1. For example, in table 2 the 3σ-clipping approach gives the best fit to the 1:1 line, but is far from the best method for estimation of the mass function. It seems the less galaxies removed from the cluster, the better is the fit to the 1:1 line. This does obviously not coincide with the results of the mass function estimates. However it indicates that the masses derived in Wang et al. (2012) are larger in general than the masses estimated using the different interloper removal methods.

In the first analysis on the 15 clusters in section 3.1, it was seen that for clusters with too few cluster members (< 15 galaxies) after the initial velocity cut off (see section 3.2.1), the masses differed with one magnitude compared to masses in Horner et al. (1999) and Rines et al. (2003). The effect of the number of cluster members on the mass function was not examined any further, however it is clear that this is also a factor to take into consideration when discussing the systematic errors in the cluster mass estimations.

The errors are calculated using the bootstrapping technique on the mass function derived from the different interloper removal methods and the mass function from Klypin et al. (2011), and go up to 31% for both mass functions. According to Wojtak et al. (2008), whether the system is in equilibrium or if it is approximately spherically symmetric, may contribute most to the errors. But Wojtak et al. (2008) also mention that if interlopers were not removed at all, the contamination by the interlopers could become the main source of error. However, it would be very difficult to disentangle the effect of interlopers from other sources of uncertainties. A direct effect of the errors can be seen in figures 6-8, 11, 12 and 13. Here the masses exceed the limit for realistic regular clusters, $10^{15} M_{\text{sun}}$ (Ferreira 2007). For MVA5 and MVA4 the whole mass function lies above $10^{15} M_{\text{sun}}$, which most likely means that MVA4 and MVA5 takes far too many interlopers into account and must thus be rejected as interloper removal methods.

5.4 Ideas for the future

There are several important reasons for studying, analysing and finding masses of galaxy clusters and the cluster mass function. The mass of galaxy clusters play an essential role in the study of large-scale physical processes, the cosmic evolution of the intergalactic intracluster medium (ICM) and the structure and evolution of our universe. They can be used as probes of structure and galaxy formation as they retain an imprint of how they were formed. As dark matter affects clusters, they are also valuable for measuring dark matter in the universe. The number of galaxy clusters as a function of mass places one of the strongest constraints on the amplitude of mass fluctuations and on the mass density parameter, Ω_m. The present-day cluster mass function was the first observation to suggest that the standard $\Omega_m = 1$ Cold Dark Matter (CDM) model must be very biased in order to match the observed abundance of clusters (Bahcall et al. 2000). This clearly makes both mass of galaxy clusters as well as the mass function very important for future research in several fields of astronomy and astrophysics.

The work and analysis made in this thesis could be elaborated and developed in future projects connected to masses of galaxy clusters. What could be done is for example making

analysis on a larger set of clusters (> 1000), developing the interloper removal methods in this thesis as well as creating new ones and implementing more mass estimators such as the median mass or average mass estimator (Heisler et al. 1985). It would be especially interesting to develop the polyfit method approach, as it is the most complex interloper removal method in this thesis, and use more initial velocity constraints on it, not only 4000 km/s. The methods in this thesis could also be used on Euclid galaxy and cluster mock catalogs to see how good cluster mass estimates Euclid data can provide. As Euclid will have data on around 60 000 clusters, the results of a mass function based on such data will be quite promising (Laureijs et al. 2011).

6 Conclusion

The maximum velocity interloper removal method (MVA) with a velocity constraint of 3000 km/s agrees best with the mass function derived analytically in Klypin et al. (2011). This constraint is physically relevant as it yields to, using Hubble's law, a maximum cluster radii of around 40 Mpc (in the same range as the superclusters). The 2σ-clipping approach (2σ) also agrees well with the mass function in Klypin et al. (2011). However it is clear that when there is an excess of interlopers or too few member galaxies in the cluster, all three interloper removal methods give a larger uncertainty and less qualitative results. The most important and perhaps the most difficult part in estimating a mass function is choosing an interloper removal method that removes enough galaxies, not too few or too many. Removing too few galaxies seems to give an even less accurate mass estimate than if removing too many. MVA4 and MVA5 are examples of two interloper removal methods that must be rejected due to an excessive amount of interlopers included in the cluster. Comparing to previous work the 3σ also seem to include too many interlopers and is less accurate when determining cluster masses than the MVA.

There are several good reasons for continuing the analysis and work in finding a cluster mass function, for example the implications it has on the mass density parameter, the study of dark matter and the importance it has on many other fields in astronomy and astrophysics.

Abbreviations

H_0	Hubble constant
M_{p}	Projected mass
M_{sun}	The mass of the Sun, $1.99 \cdot 10^{30}$ kg
M_{v}	Virial mass
$n\sigma$	σ interloper removal method where n is 2, 2.5 or 3.
A	Abell
BCG	Brightest Cluster Galaxy
CDM	Cold Dark Matter
Dec	Declination
DVC2	Different velocity criteria interloper removal method with an initial velocity constraint of 2000 km/s
GMBCG	Gaussian Mixture Brightest Cluster Galaxy
LRG	Luminous Red Galaxies
MF	Mass function
MVAn	Maximum velocity approach for interloper removal, n is 1.5, 2, 2.5, 3, 4, 5 which stand for 1500 km/s, 2000 km/s, 2500 km/s, 3000 km/s, 4000 km/s or 5000 km/s initial maximum velocity criteria.
MVGAn	Maximum velocity gap interloper removal approach where n is 70, 400, 500, 700 which stand for 70 km/s, 400 km/s, 500 km/s or 700 km/s velocity gap.
PM	Polyfit interloper removal method
RA	Right ascension
SDSS	Sloan Digital Sky Survey

References

Abazajian, K. N., Adelman-McCarthy, J. K., Agüeros, M. A., et al. 2009, ApJ, 2

Bahcall, N. A., Dong, F., Bode, P., et al. 2000, A&A

Böhringer, H. & Werner, N. 2010, A&A, 18, 127

Bolzonella, M., Miralles, J.-M., & Pello, R. 2000, A&A

Deng, X., He, J., & Song, J. 2007, Chin. J. Phys., 45

Diaconis, P. & Efron, B. 1983, A&A, 83

Dibai, E. A., Tsitsin, F. A., & Sharov, A. S. 1959, Sov. Astron., 4, 628

Ferreira, D. D. 2007, Master's thesis, University of Copenhagen, Denmark

Hao, K., McKay, T. A., Koester, B., et al. 2010, ApJ, 3

Harrison, E. R. 1974, ApJ, 191, L51

Heisler, J., Tremaine, S., & Bahcall, J. N. 1985, ApJ, 298, 8

Horner, D. J., Mushotzky, R. F., & Scharf, C. A. 1999, ApJ, 520, 78

Klypin, A. A., Trujillo-Gomez, S., & Primack, J. 2011, ApJ, 740, 102

Laureijs, R., Amiaux, J., Arduini, S., et al. 2011, ESA/SRE, 12

Mamon, G. A., Biviano, A., & Murante, G. 2010, A&A, 3

Perea, J., Del Olmo, A., & Moles, M. 1990, Ap&SS, 170, 347

Rines, K., Geller, M. J., Kurtz, M. J., & Diaferio, A. 2003, ApJ, 126, 2152

Sheth, R. K. & Tormen, G. 2001, ApJ, 1

Tinker, J., Kravtsov, A. V., Klypin, A., et al. 2008, ApJ, 688, 709

Tittley, E. R. & Couchman, H. M. P. 1999, ApJ, 1

Wang, L., Yang, X., Luo, W., et al. 2012, ApJ, 2

Weisstein, E. W. 2012, Spherical Trigonometry From MathWorld—A Wolfram Web Resource, last visited on 8/5/2012

Wojtak, R., Lokas, E. L., Mamon, G. A., et al. 2008, A&A, 6813